A unified computational and experimental approach to determine laser safety of liver tissue

Junior Arroyo[a], Jiaxin Zhang[b], and Muyinatu A. Lediju Bell[a,b,c]

[a]Johns Hopkins University, Department of Biomedical Engineering, Baltimore, Maryland, United States
[b]Johns Hopkins University, Department of Electrical and Computer Engineering, Baltimore, Maryland, United States
[c]Johns Hopkins University, Department of Computer Science, Baltimore, Maryland, United States

ABSTRACT

Photoacoustic imaging has promising potential to be integrated into surgical guidance systems. However, this integration can potentially be limited by biosafety concerns. While laser safety guidelines exist for skin, corneal, and retinal tissue, there are no guidelines for liver tissue. We introduced the first known numerical simulation approach to determine laser safety for liver tissue and present a novel microscopy analysis framework to validate performance. Our innovative approach integrates Monte Carlo simulations of laser-tissue interaction followed by COMSOL modeling for necrosis prediction. These predictions are demonstrated with pulsed laser exposure using 30 mJ and 73 mJ laser energies with an optical wavelength of 750 nm administered for exposure durations of 1, 10, and 20 minutes. Empirical validations were performed with necrosis values quantified from immunohistochemical sections of swine liver exposed to the same laser conditions *in vivo*. These necrosis predictions deviated from quantitative histological results by 0.01% to 8.1%. The presented approach provides a promising alternative to traditional, time-intensive experimental methods to otherwise determine laser safety guidelines, which is expected to translate to multiple tissues and laser properties.

Keywords: photoacoustic imaging, laser safety, numerical simulation, microscopy, single-cell segmentation, necrosis

1. INTRODUCTION

Laser safety is an important biohazard consideration to ensure patient safety during photoacoustic interventional guidance. The American National Standards Institute provides guidelines to determine the maximum permissible exposure (MPE), representing the maximum allowable pulse energy per unit area to prevent adverse biological effects.[1] While these guidelines exist for human skin and retinal tissue, they are not defined for internal tissues, such as the liver. Considering these available options, the MPE for skin is typically used as a reference during interventional guidance testing,[2] but this assumption can unnecessarily limit the maximum applied exposure and consequently limit the photoacoustic image contrast.[3,4]

Experiments were previously conducted to determine appropriate parameters to minimize and control the risk of tissue damage to liver tissue. Kempski *et al.*[4] demonstrated that the minimum energy required for optimal visualization of hepatic vessels was 30 mJ (153 mJ/cm^2 fluence), which exceeds the MPE limit for skin. Although 80 minutes of laser exposure with varying laser energies (including energies that exceeded 30 mJ) and excessive tissue handling caused liver tissue to experience hemorrhage, inflammation, and necrosis, after reducing the exposure time to at most 20 minutes and maintaining the energy at 30 mJ, Huang *et al.*[3] demonstrated the absence of necrosis. In both reports, the pulse duration was 5 ns, the pulse repetition frequency was 10 Hz, the laser wavelength was 750 nm, and histological features were qualitatively graded from H&E-stained sections.

Herein, we summarize both quantitative and qualitative assessments of laser-induced tissue necrosis using swine liver samples. A novel simulation framework,[5] summarized in Fig. 1, was deployed to predict tissue necrosis based on input laser parameters, including incident energy, beam diameter, wavelength, and exposure time. The resulting predictions were validated with *in vivo* experiments conducted using matching laser parameters. In

Optical Interactions with Tissue and Cells XXXVI, edited by Norbert Linz, Joel N. Bixler, Alex J. Walsh, Proc. of SPIE Vol. 13317, 1331704 · © 2025 SPIE
1605-7422 · doi: 10.1117/12.3044908

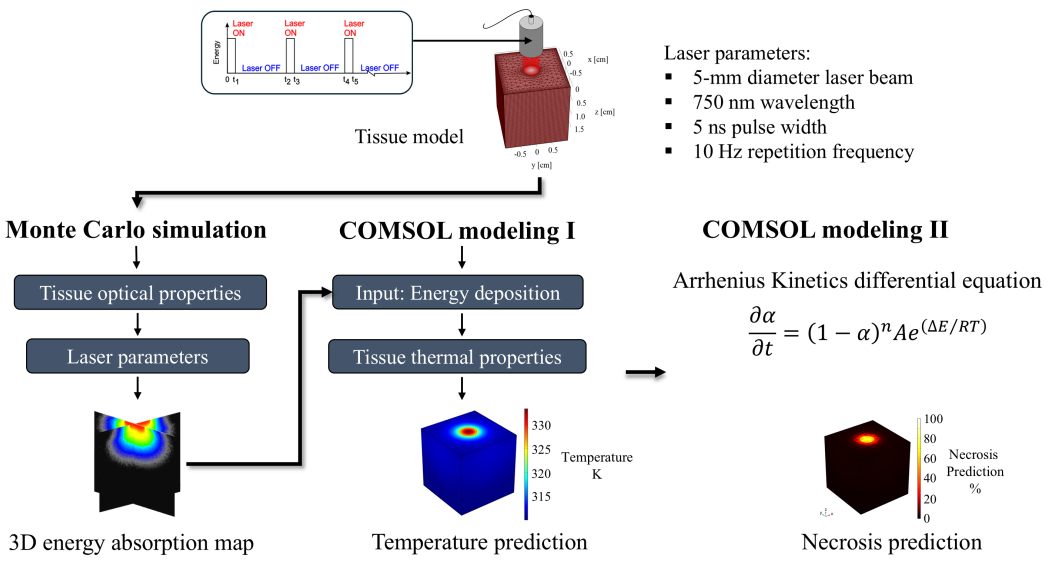

Figure 1: Graphical summary of our novel simulation framework. Sequential Monte Carlo simulations and COMSOL modeling were used to predict the temperature distribution within a tissue model, to ultimately predict the associated necrosis, expressed as a percentage of necrotic cells at the surface of the tissue model.

addition, a quantitative method, previously introduced to assess necrosis from digitized immunohistochemistry (IHC) sections,[5] was implemented for comparison to our predictive modeling approach.

2. METHODS

2.1 Simulation methods

A 20×20×20 mm^3 homogeneous swine liver tissue block was modeled, followed by simulated exposure to laser light from a 5 mm-diameter pulsed laser source delivering an optical wavelength of 750 nm, 5 ns pulse duration, and 10 Hz pulse repetition frequency, for durations of 1, 10, and 20 minutes. Two energies were independently delivered (30 mJ and 73 mJ). The lower energy level is not expected to damage liver tissue,[3] while the higher energy level is expected to induce necrosis[5] after 20 minutes of laser exposure.

As summarized in Fig. 1, three-dimensional (3D) Monte Carlo simulations[6] were implemented to model tissue-photon interactions and obtain a 3D energy absorption map. Then, the Pennes Bioheat transfer equation was employed using COMSOL Multiphysics 6.1[7] simulations to model thermal conduction in a hyperthermia process, resulting in temperature predictions. The Arrhenius kinetics model was then implemented to quantify thermal damage, resulting in the reporting of necrosis predictions as a percentage of the laser-exposed tissue surface.

The cubic model for bioheat transfer simulations was divided into three domains for mesh conversion: the region directly exposed to the laser beam, the surface exposed to the laser beam, and the remainder of the model. The first domain used triangular elements with a maximum element size of 2 mm, the second domain used triangular elements with a maximum element size of 3 mm, and the third domain was meshed with quadrilateral elements with a maximum size of 3 mm, which generated hexahedral elements for the volumetric mesh. The laser-exposed surface exchanged heat with the environment based on free convection in air. The remaining five surfaces were kept at constant temperature. Additional details about the pulsed laser heat source definition, the differential equation of the Arrhenius kinetic model, the fraction of necrotic tissue equation, and the optical and thermal parameters, are available in our recently published journal paper.[5]

2.2 Experiments

The following study was approved by the Johns Hopkins University Institutional Animal Care and Use Committee and previously summarized by Arroyo *et al.*[5] A laparotomy was performed on the abdomen of a female Yorkshire swine (36 to 40 kg) to access and expose the left lateral liver lobe. A 5 mm-diameter fiber bundle was connected to a Phocus Mobile laser containing an internal power meter (Opotek, Carlsbad, California) to deliver laser energy to three locations on the surface of the exposed *in vivo* liver lobe: (1) 73.0 mJ mean energy was delivered for 20 minutes to a cranial position on the lobe, (2) 72.5 mJ mean energy was delivered for 10 minutes to a caudal position, and (3) 73.6 mJ was delivered for 1 minute to a more caudal position. The optical wavelength was 750 nm, delivered with a 5 ns pulse width at a pulse repetition frequency of 10 Hz. Tissue marking dye was immediately applied to each region after laser application. The swine was then euthanized, and the entire left lateral liver lobe was removed from the abdomen to excise the marked regions, which were immediately fixed in a 10% formalin solution.

To prepare the excised samples for analysis, these samples were first embedded in paraffin, then placed in a microtome with the irradiated surface oriented approximately parallel to the microtome blade. Each sample was sectioned into 250 sections with a section thickness of 4 µm. To perform IHC analysis on sections with 40 µm separation, one section in every group of 10 consecutive sections was stained with an antibody specific to cleaved Caspase-3 (1:1000 dilution ratio). These 25 stained sections were used to identify necrotic areas resulting from prolonged laser exposure. In addition, one section was extracted from a 928 µm depth (to ensure that the entirety of the relevant tissue cross section was accurately represented), then stained with Hematoxylin and Eosin (H&E) for qualitative necrosis grading.

2.3 Quantitative thermal damage assessment

Individual IHC sections were digitized at 40x magnification using a Hamamatsu NanoZoomer S210 to generate NDPI files. The NDPITools Plugin Bundle of ImageJ[8] divided each IHC section into mosaic of adjacent JPEG images, encoding color information using Red-Blue-Green (RGB) channels. A visual inspection of the digitized IHC section (Fig. 2) revealed the presence of cleaved Caspase-3-positive cells stained in intense brown and cleaved Caspase-3-negative cells stained in intense blue. The irradiated region showed reduced cell density, few brown cells, and a similar density of blue cells compared to non-irradiated areas.

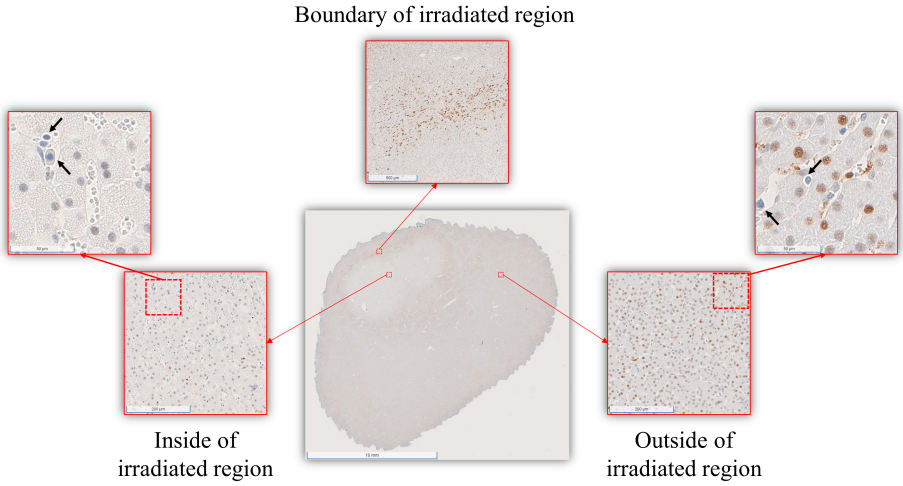

Figure 2: Visual inspection of a representative digitized IHC section. Blue cells are pointed out by arrows. The overall cell density was greater outside rather than inside the irradiated area. The boundary of the irradiated area presented a high concentration of brown cells. Reproduced from Arroyo *et al.*[5]

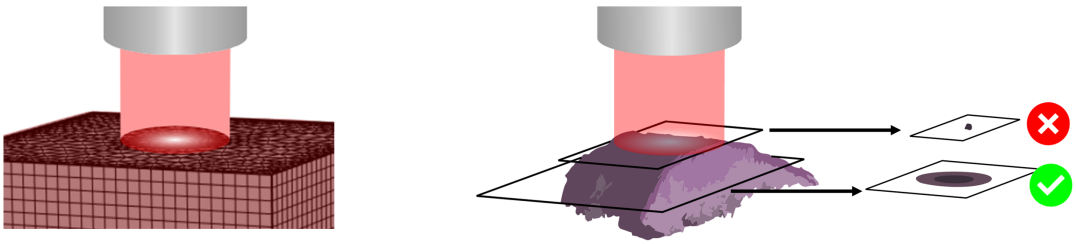

(a) (b)

Figure 3: Laser safety assessment was conducted by analyzing the thermal impact of laser light at the tissue surface. Direct comparison between simulation and experimental results was challenging due to differences in tissue geometry, as (a) the liver tissue model has a flat surface, while (b) the *in vivo* liver sample has a curved surface. Superficial sections from the liver samples that were too small to depict the entire laser-exposed area were excluded. Instead, the most superficial section that included both the entire laser-exposed area along with the adjacent non-exposed tissue was selected for validation.

An Attention U-Net,[9] implemented in Python 3.9.15 in a Jupyter Notebook, was used to segment cells from the digitized IHC sections. Individual segmented cells were analyzed for classification into blue or brown cells. A cell was categorized as either brown or blue if its RGB components satisfied the conditions $60 \leq \mathrm{R} \leq 210$, $\mathrm{G} \leq 151$, and $\mathrm{B} \leq 130$ or $150 \leq \mathrm{R} \leq 186$, $\mathrm{G} \geq 155$, and $\mathrm{B} \geq 160$, respectively. This procedure was performed using MATLAB R2023a (Mathworks, Natick, Massachusetts) software. To quantify local necrosis from the IHC sections, the spatial distribution of blue and brown cells were modeled as an exponential decay, as follows:

$$\text{Necrosis} = \Gamma\, e^{-k\rho} \times 100\% \tag{1}$$

where Γ and ρ represent fractions of the areas of blue and brown cells, and $k = 100$ enables us to define ρ as a fraction rather than the percentage that $k\rho$ represents. The fractions were defined as:

$$\Gamma = \frac{\text{blue cell area}}{\text{blue cell area} + \text{brown cell area}}, \tag{2}$$

and

$$\rho = \frac{\text{brown cell area}}{\text{total patch area}} \tag{3}$$

where the total patch area is 200 µm× 200 µm, which was selected to display approximately 20-200 cells per patch (i.e., the cells were approximately 5-10 µm in diameter). When there are no brown cells within the irradiated region, the model presented in Eqs. (1)-(3) successfully achieved Γ=1, ρ=0, and 100% necrosis, with a lower necrosis percentage achievable when brown cells are present. The multiplicative exponential term, $e^{-k\rho}$, was introduced to proportionally scale the fraction of blue cells (i.e., Γ) present by the local density of brown cells (i.e., ρ). This exponential term produced a steep change in the necrosis percentage near the boundary of the irradiated region. Necrosis quantification was conducted for the 25 IHC sections, and the resulting necrosis maps were placed in a common coordinate frame using rigid registration. A two-stage filtering process was implemented to remove artifacts from the registered necrosis maps.[5]

2.4 Comparison of predicted and experimental thermal damage

Simulation predictions were compared to experimental results, based on necrosis observed at the laser-tissue interface (i.e., where the tissue experiences the most direct laser exposure). To account for the geometric differences between the curved liver samples and the flat simulated tissue model (Figure 3), IHC sections were selected at depths of 0, 280, and 160 µm for 1, 10, and 20-minute irradiation times, respectively. These sections represented the shallowest depths that fully displayed the irradiated region and its adjacent non-irradiated area. Absolute errors between predicted and experimental necrosis percentages were calculated.

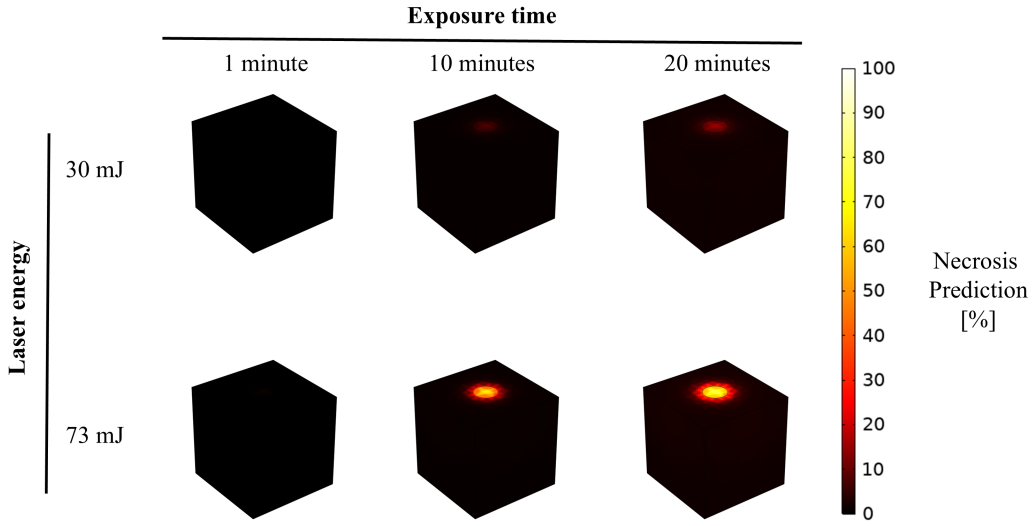

Figure 4: Necrosis predictions for two energies independently delivered (i.e., 30 mJ and 73 mJ) with exposure durations of 1, 10, and 20 minutes.

3. RESULTS AND DISCUSSION

3.1 Thermal damage predictions

Fig. 4 shows volumetric necrosis predictions for different exposure times using laser energies of 30 mJ and 73 mJ. At the center of the laser-exposed area, the induced damage slowly progressed during the first minute of irradiation, resulting in a necrotic tissue percentage of 1.23%. Extending the laser exposure to 10 minutes led to a necrotic tissue percentage of 66.23%. Following 20 minutes of laser irradiation, the necrotic tissue percentage escalated to 76.84%. For a laser energy of 30 mJ, the necrotic tissue percentages were 0.03%, 7.49%, and 15.05% for laser exposure durations of 1 minute, 10 minutes, and 20 minutes, respectively.

3.2 Empirical thermal damage assessment

Figure 5 shows thermal damage assessment results for a representative digitized IHC section irradiated for 10 minutes. The IHC section was digitized (Fig. 5(a)) and divided into a mosaic composed of 16384 JPEG images (Fig. 5(b)). Cells from individual JPEG images were segmented (Fig. 5c) using an Attention U-Net (0.97 DSC, 0.94 IoU, 0.99 recall, and 0.95 precision). The segmentation mask of the full section (Fig. 5(d)) shows the spatial distribution of blue and brown cells. The local necrosis map (Fig. 5e) computed using Eq. 1 shows a round central region surrounded by areas of variable necrosis percentage. The necrosis values corresponding to the irradiated region were preserved after filtering the artifacts (Fig. 5(f)).

Figure 6 shows necrosis maps for the swine liver samples exposed with mean energies of 73.6 mJ, 72.5 mJ, and 73.0 mJ for 1, 10, and 20 minutes, respectively. These necrosis maps correspond to tissue sections extracted at depths of 0, 280, and 160 µm below the tissue surface for the 1, 10, and 20-minute irradiation times, respectively. There are no signs of cell disruption when the laser was applied for 1 minute, yielding 0% necrosis percentage. Laser application for 10 minutes caused moderate disruption of cells, resulting in a mean necrosis percentage of 66.22%. Laser exposure for 20 minutes disrupted cells in the illuminated area, yielding a mean necrosis percentage of 84.94%.

Table 1 summarizes the simulation and experimental histopatholgical results. For the laser energy of approximately 30 mJ, qualitative necrosis grading were derived from previously reported results from 35 liver samples.[3] with no quantitative histopathological available (indicated as N/A). For the laser energy of approximately 73 mJ, deviations between necrosis predictions and necrosis quantification from experimental results were 1.23%, 0.01%, and 8.1% for 1, 10, and 20 minutes of laser exposure, respectively.

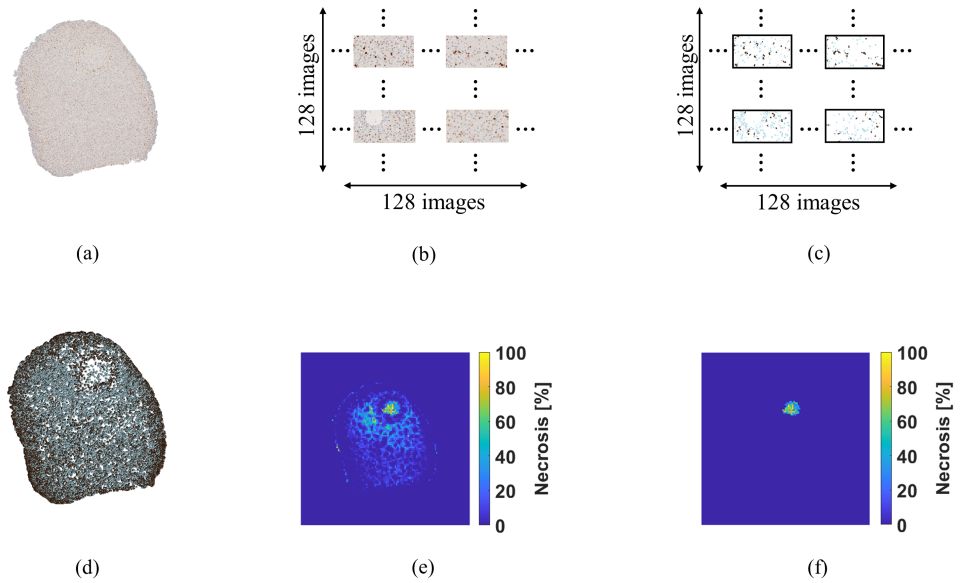

Figure 5: Image processing workflow for necrosis quantification of IHC sections: (a) IHC section, (b) mosaic of 16384 RGB images, (c) segmentation, (d) blue and brown cells segmentation, (e) necrosis map, and (f) filtered map. Reproduced from Arroyo et al.[5]

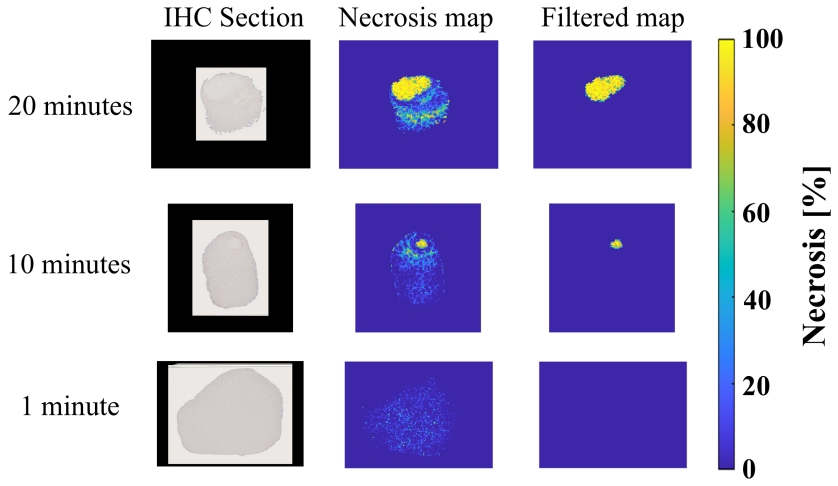

Figure 6: IHC section, initial necrosis map, and filtered necrosis map for swine liver samples irradiated for 1, 10, and 20 minutes. Reproduced from Arroyo et al.[5]

Fig. 7 graphically summarizes our assessments of laser safety based on the presented results. Considering that a predicted necrosis of 15.05% corresponded to the absence of visible liver necrosis, whereas a predicted necrosis of 66.23% corresponded to visible necrosis, it is reasonable to assume that the damage threshold resides within the 15.05% - 66.23% necrosis prediction range. Therefore, we assess liver imaging using a 750 nm wavelength laser at 5 ns pulse duration, 10 Hz pulse repetition frequency, and 30 mJ laser energy (152.79 mJ/cm^2 fluence) as safe for up to 20 minutes. At 73 mJ laser energy (371.79 mJ/cm^2 fluence), no necrosis (1.23% *in silico*, 0% *in vivo*) ocurred within one minute of exposure. We assess larger, exposure durations of 10 and 20 minutes as unsafe, due to 66.23% and 76.84% necrosis, respectively, measured *in silico* and the corresponding 66.22% to 84.94% necrosis, respectively, measured with *in vivo* liver.

Table 1: Comparison of simulated predictions, qualitative necrosis grading, and quantitative histopathological assessment of necrosis from IHC sections in swine liver samples irradiated with approximately 30 mJ and 73 mJ laser energy for 1, 10, and 20 minutes. Qualitative analysis graded necrosis as absent (- -), minimal (-), mild (+), moderate (++), and severe (+++) based on H&E stains.

Energy	Laser Time (minutes)	Necrosis grading	Necrosis prediction (%)	IHC (%)
30 mJ	1	- -	0.03	N/A
	10	- -	7.49	N/A
	20	- -	15.05	N/A
73 mJ	1	- -	1.23	0
	10	+	66.23	66.22
	20	+++	76.84	84.94

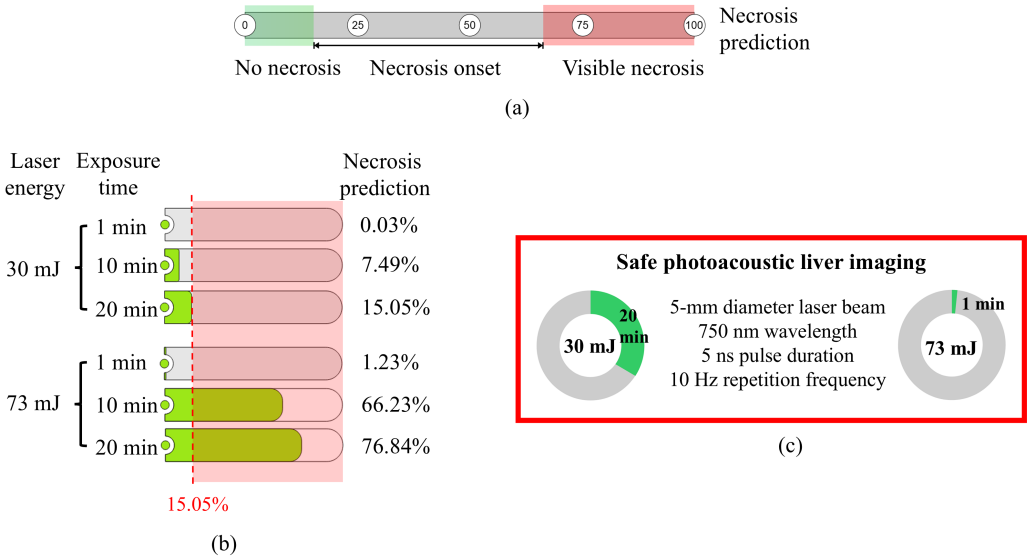

Figure 7: (a) Bar plot showing the relationship between necrosis prediction values and histology-based necrosis grading. A region with no visible necrosis corresponds to necrosis prediction values ranging from 0 to 15.05%, while visible necrosis values aligns with necrosis prediction values ranging from 66.23% to 100%. (b) Bar plot summarizing the results from Table 1, depicting the necrosis prediction for two laser energy levels and three different exposure times. A necrosis prediction threshold of 15.05%, indicative of no visible necrosis, can be used to guide the selection of optimal laser parameters to prevent thermal damage. (c) Graphical illustration of optimal laser parameters (supported by our study results) offering safe photoacoustic liver imaging.

4. CONCLUSION

This paper summarizes our pioneering work to quantify the thermal effects of laser exposure to *in vivo* liver tissue, demonstrating 0.01% to 8.1% simulated necrosis deviations from experimental results. Our novel microscopy analysis framework based on immunohistochemistry results successfully provided the first known quantitative necrosis assessment for swine liver across multiple exposure durations. Overall, the presented work highlights the benefits of a simulation framework integrating Monte Carlo simulations and COMSOL thermodynamic modeling to estimate laser-induced necrosis percentage. The framework predictions are well-aligned with the experimental validation results. These results are promising to provide tissue-specific MPE guidelines, relevant to multiple laser-based optical and photoacoustic surgeries and interventions. In addition, this approach is promising to develop tissue-specific safety guidelines for photoacoustic imaging and optics-based imaging technologies aimed at maximizing signal-to-noise ratios while ensuring patient safety.

ACKNOWLEDGMENTS

This work is supported by the Alfred P. Sloan Research Fellowship in Physics, by the Johns Hopkins University Provost's Catalyst Award, and by the National Science Foundation (NSF) under NSF CAREER Award No. ECCS-1751522, NSF SCH Award No. IIS-2014088, and NSF Alan T. Waterman Award No. IIS-2431810. We thank Jessica Izzi and the staff of the Johns Hopkins Medicine Research Animal Services for animal care and surgery support. We additionally acknowledge the support of shared tissue preparation and histopathology resources made possible through NIH P30 CA006973.

REFERENCES

[1] ANSI, [*American National Standard for Safe Use of Lasers*], Laser Institute of America (2014).

[2] Bell, M. A. L., "Photoacoustic imaging for surgical guidance: principles, applications, and outlook," *Journal of Applied Physics* **128**(6), 060904 (2020).

[3] Huang, J., Wiacek, A., Kempski, K. M., Palmer, T., Izzi, J., Beck, S., and Bell, M. A. L., "Empirical assessment of laser safety for photoacoustic-guided liver surgeries," *Biomedical Optics Express* **12**(3), 1205–1216 (2021).

[4] Kempski, K. M., Wiacek, A., Graham, M., González, E., Goodson, B., Allman, D., Palmer, J., Hou, H., Beck, S., He, J., and Bell, M. A. L., "In vivo photoacoustic imaging of major blood vessels in the pancreas and liver during surgery," *Journal of Biomedical Optics* **24**(12), 121905 (2019).

[5] Arroyo, J. J., Sharma, A., Zhang, J., and Bell, M. A. L., "Predictive model for laser-induced tissue necrosis with immunohistochemistry validation," *Biophotonics Discovery* **1**(2), 025003–025003 (2024).

[6] Fang, Q. and Boas, D. A., "Monte carlo simulation of photon migration in 3d turbid media accelerated by graphics processing units," *Optics Express* **17**(22), 20178–20190 (2009).

[7] "Comsol multiphysics v. 6.1." https://www.comsol.com. COMSOL AB, Stockholm, Sweden. 2022.

[8] Deroulers, C., Ameisen, D., Badoual, M., Gerin, C., Granier, A., and Lartaud, M., "Analyzing huge pathology images with open source software," *Diagnostic Pathology* **8**, 1–8 (2013).

[9] Oktay, O., Schlemper, J., Folgoc, L. L., Lee, M., Heinrich, M., Misawa, K., Mori, K., McDonagh, S., Hammerla, N. Y., Kainz, B., et al., "Attention u-net: Learning where to look for the pancreas," *arXiv preprint arXiv:1804.03999* (2018).